# High-precision half-life measurements for the superallowed Fermi $\beta^+$ emitter $^{18}$Ne

A. T. Laffoley,[1,*] C. E. Svensson,[1] C. Andreoiu,[2] G. C. Ball,[3] P. C. Bender,[3] H. Bidaman,[1] V. Bildstein,[1] B. Blank,[4] D. S. Cross,[2] G. Deng,[1] A. Diaz Varela,[1] M. R. Dunlop,[1] R. Dunlop,[1] A. B. Garnsworthy,[3] P. E. Garrett,[1] J. Giovinazzo,[4] G. F. Grinyer,[5] J. Grinyer,[5] G. Hackman,[3] B. Hadinia,[1] D. S. Jamieson,[1] B. Jigmeddorj,[1] D. Kisliuk,[1] K. G. Leach,[1,2,3] J. R. Leslie,[6] A. D. MacLean,[1] D. Miller,[3] B. Mills,[3] M. Moukaddam,[3] A. J. Radich,[1] M. M. Rajabali,[3] E. T. Rand,[1] J. C. Thomas,[5] J. Turko,[1] C. Unsworth,[3] and P. Voss[2]

[1]*Department of Physics, University of Guelph, Guelph, Ontario N1G 2W1, Canada*

[2]*Department of Chemistry, Simon Fraser University, Burnaby, British Colombia V5A 1S6, Canada*

[3]*TRIUMF, 4004 Wesbrook Mall, Vancouver, British Columbia V6T 2A3, Canada*

[4]*Centre d'Etudes Nucléaires de Bordeaux Gradignan, IN2P3/CNRS - Université de Bordeaux, 33175 Gradignan, France*

[5]*Grand Accélérateur National d'Ions Lourds (GANIL), CEA/DSM-CNRS/IN2P3, Bvd Henri Becquerel, 14076 Caen, France*

[6]*Department of Physics, Queen's University, Kingston, Ontario K7L 3N6, Canada*

(Received 1 June 2015; published 6 August 2015)

The half-life of the superallowed Fermi $\beta^+$ emitter $^{18}$Ne has been determined via two high-precision $\beta$ counting experiments at TRIUMF's Isotope Separator and Accelerator facility. Using two different $4\pi$ continuous-flow gas-proportional counters, two independent measurements were made, yielding a weighted average of $T_{1/2} = 1.66400^{+0.00057}_{-0.00048}$ s, which is consistent with but approximately 2 times more precise than a previous high-precision measurement based on $\gamma$-ray counting. The present work achieves $\pm 0.034\%$ precision for the $^{18}$Ne half-life and will enable the inclusion of $^{18}$Ne among the set of precisely measured superallowed Fermi $\beta$-decay $ft$ values once improved measurements are made for its $Q$ value and superallowed branching ratio. As a test of systematic uncertainties, the half-life of $^{23}$Ne was measured and the world average has been improved, by a factor of 1.7, to $37.148 \pm 0.032$ s.

DOI: 10.1103/PhysRevC.92.025502 PACS number(s): 23.40.−s, 21.10.Tg, 24.80.+y, 27.20.+n

## I. INTRODUCTION

The study of superallowed Fermi $\beta$ transitions between nuclear isobaric analog states of spin $J^\pi = 0^+$ provides demanding, and fundamental, tests of the properties of the electroweak interaction. In particular, high-precision measurements of the $\beta$-decay $ft$ values for superallowed Fermi $\beta$ emitters with isospin $T = 1$ have been used to validate the conserved vector current (CVC) hypothesis to better than 12 parts in $10^5$ and provide the most precise determination of $V_{ud}$, by far the most precisely determined element of the Cabibbo-Kobayashi-Maskawa (CKM) quark mixing matrix [1–3]. Limits on the unitarity of the CKM matrix are currently tested most precisely using the top row of the matrix. Despite being determined to a precision of $\pm 0.022\%$ by the superallowed data, $V_{ud}$ accounts for approximately 95% of the top row unitarity sum and hence contributes a comparable absolute uncertainty to the unitarity test as $V_{us}$, which is currently determined with an order of magnitude less precision, while the contribution of $V_{ub}$ to the unitarity sum is negligible [1]. Therefore, determination of $V_{ud}$ with high precision, specifically through improved measurements of the $ft$ values of superallowed Fermi $\beta$ emitters, remain critical for improving the test of CKM unitarity and the limits this test sets on new physics beyond the standard model.

Theoretical corrections must be applied to the experimentally determined $ft$ values for the superallowed Fermi $\beta$ emitters in order to obtain nucleus independent "corrected" $\mathcal{F}t$ values [1]:

$$\mathcal{F}t = ft(1+\delta_R')(1+\delta_{NS}-\delta_C) = \frac{K}{2G_V^2\left(1+\Delta_R^V\right)}, \quad (1)$$

where $K/(\hbar c)^6 = 2\pi^3\hbar \ln 2/(m_e c^2)^5 = 8120.2776(9) \times 10^{-10}$ GeV$^{-4}$s, $G_V$ is the vector coupling constant for semileptonic weak interactions, $\Delta_R^V$ is the transition-independent component of the radiative correction, $\delta_R'$ and $\delta_{NS}$ are the transition-dependent components of the radiative correction, and $\delta_C$ is the isospin-symmetry-breaking correction. Given experimental measurements of the $ft$ values, the weak vector coupling constant $G_V$, and ultimately $V_{ud}$, can be extracted from Eq. (1). In the determination of $V_{ud}$, the transition-independent component of the radiative correction, $\Delta_R^V$, currently contributes 0.018% of the total 0.022% uncertainty [1]. Improvement in the calculation of $\Delta_R^V$ in the near future is unlikely and remains a problem strictly for theory [4]. Of the remaining sources of uncertainty, 0.005% can be considered experimental in origin, while 0.011% comes from the nuclear-structure-dependent radiative and isospin-symmetry-breaking corrections ($\delta_C$,$\delta_{NS}$,$\delta_R'$) [1]. In particular, the $\delta_C$ corrections, which range from 0.2 to 1.6% for the 14 high-precision superallowed $\mathcal{F}t$ cases, are particularly sensitive to both the theoretical model employed and, for shell-model calculations, the model space chosen and have been the subject of intense scrutiny by a wide variety of theoretical and semiempirical techniques over the past two decades [1,5–17].

Much current interest lies in the set of superallowed decays with $T_Z = -1$ parents, as the $\delta_C$ corrections are,

*alaffole@uoguelph.ca

 

in general, larger than those for the $T_z = 0$ parents of the same mass. This arises naturally due to the larger difference in proton and neutron separation energies that serves to increase the radial-overlap mismatch between the proton and neutron wave functions in the parent and daughter nuclei. However, high-precision measurements of the $ft$ values for these decays are, in general, more challenging than for the $T_z = 0$ parents, due both to the fact that they are further from stability, where production of beams becomes more difficult, and their daughter nuclei are in general also $\beta$ unstable and give rise to unwanted but unavoidable time-dependent $\beta$-decay backgrounds. In addition, for most cases, there is strong Gamow-Teller feeding to low-lying $J^\pi = 1^+$ states in the odd-odd $N = Z$ daughter nucleus that competes with the superallowed transition, making the superallowed branching ratio difficult to measure precisely. These experimental challenges are evidenced by the absence of high-precision $ft$ values for the majority of the $T_z = -1$ emitters beyond $^{10}$C and $^{14}$O, for which the daughter nuclei are stable. Recent experimental efforts, in combination with extensive simulation work, have, however, demonstrated that these challenges can be overcome [18–21].

The specific case of the superallowed decay of the $T_Z = -1$ parent $^{18}$Ne provides another excellent candidate for investigating the theoretical description of isospin symmetry breaking as the varying models exhibit a large range of potential $\delta_C$ corrections, ranging from 0.27% to 1.41% [1,8,10,11,16]. Presently, the standard in this field is set by the $\delta_C$ calculations of Towner and Hardy, with radial wave functions calculated using a Woods-Saxon potential constrained to experimental binding energies and nuclear charge radii [8]. These calculations yield a value of $\delta_{C2}(^{18}\text{Ne}) = 0.405(25)\%$ [1] for the radial overlap component of isospin symmetry breaking but when evaluated using Hartree-Fock radial wave functions (also by Towner and Hardy [13]) they yield a smaller correction of $\delta_{C2}(^{18}\text{Ne}) = 0.205(55)\%$. These two models thus disagree in the calculation of $\delta_{C2}$ at the level of 0.20(6)%, or $3.3\sigma$, the largest such discrepancy for any of the 20 superallowed $0^+ \rightarrow 0^+$ Fermi $\beta$ transitions with $ft$ values experimentally measured to better than 3%. Thus, a high-precision $ft$ value determination for $^{18}$Ne superallowed decay would provide a particularly stringent test of the differences between these theoretical models.

In order to be included among the high-precision cases, the precision of the branching ratio, half-life, and $Q$ value for $^{18}$Ne superallowed decay all must be improved. In anticipation of an updated branching ratio measurement [22], high-precision half-life measurements for $^{18}$Ne achieved the required $\leqslant 0.05\%$ precision with the 14 precisely measured superallowed Fermi $\beta$ emitters used in the evaluation of $V_{ud}$ [1]. By performing half-life measurements that directly count the emitted $\beta^+$ particles using $4\pi$ gas proportional counters with almost 100% detection efficiency, as well as producing $^{18}$Ne radioactive beams with reduced contamination from the daughter nucleus, $^{18}$F, we report here a measurement of the $^{18}$Ne half-life with $\pm 0.034\%$ precision, more than twice the precision achieved in a recent $\gamma$-ray counting experiment [23].

## II. EXPERIMENT

Two separate experiments were performed at TRIUMF's Isotope Separator and Accelerator (ISAC) facility. For both experiments, a 70-$\mu$ A beam of 480-MeV protons impinged on a SiC target,[1] inducing spallation reactions whose products diffused from the target and were ionized using a forced electron-beam-induced arc discharge (FEBIAD) ion source. A mass separator was used to select a beam of singly ionized $A = 18$ products, including the primary beam of $^{18}$Ne as well as a contaminant of its long-lived radioactive daughter $^{18}$F ($T_{1/2} = 109.73(2)$ min [24]), which were delivered to the experimental facilities.

During the first experiment, performed in August 2013, the target was coupled to the ion source via a cold-transfer line. This provided a temperature gradient between the $\sim$2500 °C target and a $\sim$100 °C copper block prior to the ion source and was designed to suppress the transmission of contaminant activities, such as $^{18}$F, relative to noble gases such as $^{18}$Ne. When using the cold-transfer line with the SiC target and FEBIAD ion source, the $^{18}$Ne intensity was reduced by a factor of $\sim$10 while the $^{18}$F contaminant was suppressed to undetectable levels. The resulting $A = 18$ beam with an energy of 30 keV was delivered to the experiment at a rate of approximately $4.7 \times 10^4$ $^{18}$Ne/s. In the second experiment, performed in July 2014, the cold-transfer line was not used and beam rates of $4.8 \times 10^5$ $^{18}$Ne/s and $1.1 \times 10^6$ $^{18}$F/s were achieved and delivered to the experiment at an energy of 20 keV. Both experiments were performed in a cycling mode. The low-energy beam was implanted in an aluminized Mylar tape to build up a source of $^{18}$Ne. Once a source of sufficient activity was collected, the beam was deflected at the mass separator and the tape was moved to position the sample at the center of the $4\pi$ gas proportional counter. The activity of the $^{18}$Ne sample was then counted for 40 s ($\approx$24 half-lives) and the cycle was repeated. A single run consisted of approximately 75 cycles, and between runs experimental conditions were varied in order to investigate possible systematic effects.

### Gas proportional counters

In both experiments a $4\pi$ continuous-flow gas proportional counter was used to detect the $\beta$ particles. The first of these detectors, used in the August 2013 experiment, has been used to perform high-precision half-life measurements for several decades as described, for example, in Refs. [25–28]. A second gas proportional detector, constructed as a replica of the original and colloquially named the "new counter," was used in the second experiment performed. The new counter uses a 2.16-$\mu$m Havar[2] foil as a thin window protecting the active volume from air while allowing the decaying $\beta$ particles to easily penetrate and ionize the methane gas. The anode wire used in both the counters is a gold-plated tungsten wire with a nominal radius of 6.35 $\mu$m. The only difference between the

[1] 25.52 g/cm$^2$ for the first experiment and 28.68 g/cm$^2$ for the second experiment.

[2] Made by Hamilton Precision Metals.

two detectors was the bias voltage required to operate in the plateau region, which was determined through measurements with $^{90}$Sr $\beta$ sources to be centered around 2750 V for the original counter and 2450 V for the new counter.

A significant modification to the experimental apparatus used in previous high-precision half-life measurements with the $4\pi$ gas counter at ISAC [27,28] was a new tape-transport system. A new thick-tape (T-Tape) system was commissioned specifically for use with the implantation of noble gas ions used in these experiments. The 51-$\mu$m Mylar (51 $\mu$m) tape was 2.54 cm wide and had a thick and uniform coating of 4.64 mg/cm$^2$, or 17.2 $\mu$m, of aluminum (on one side) facing the beam to ensure that all $^{18}$Ne ions were contained in the Al layer and to prevent the diffusion that occurs when noble gases are implanted in Mylar [29,30]. The center of the gas counter was positioned 27.94 cm from the beam implantation site, and the tape movement speed, controlled by a stepping motor and magnetic break, was set to approximately 38 cm/s.

As with all proportional counters, space charge can significantly affect the performance of the detector. In particular, the ion current and space charge can reduce the effective voltage within the active volume of the gas counter, resulting in a rate-dependent change in the operating conditions of the detector. To prevent this from happening, two precautions were taken: first, the gas was continually flushed through the detector at a rate of approximately 0.5 cc/min, and second, the maximum count rate within the detector was always limited to no more than 11 000 counts/s.

In both experiments, the data were processed by two independent multichannel scaler (MCS) modules and binned into 250 channels 160 ms long. Fixed, nonextendible dead times of approximately 3 and 4 $\mu$s, chosen to be much longer than the series dead time of the system, were applied to the respective MCS modules and were interchanged periodically throughout the experiment to investigate possible systematic effects.

The cycle used in each experiment was 0.5 s of ion implantation; 1.5–4.5 s of cooling (varied to keep the initial activity in the gas counter below 11 kHz); 2 s to activate the stepping motor, move the tape, and deactivate the motor; and then 40 s (or $\approx$24 $^{18}$Ne half-lives) of counting the sample before the process was repeated.

## III. ANALYSIS

Individual cycles were inspected and rejected from the final analysis if a minimum threshold on the number of $\beta$ particles detected in the cycle was not exceeded. This removed cycles during which the $^{18}$Ne beam delivery was interrupted, primarily due to interruptions in the 480-MeV proton production beam on the SiC target. The minimum threshold used was varied to test for any systematic bias in this cycle selection, as discussed further below, but for the full range of thresholds investigated the cycle selection removed between 0.2% and 3.3% of the total recorded $\beta$ decays. Once the cycle selection was performed, the data were dead time corrected on a cycle-by-cycle basis [27] before being fit using a maximum-likelihood technique that has been described in detail in previous articles [25,27,28,31].

The fit function used in the analysis included:

(i) an exponentially decaying component for the primary beam of $^{18}$Ne, with both a free initial activity and a free half-life,
(ii) a component for the grow-in and decay of the daughter nucleus $^{18}$F, with a fixed half-life and an activity coupled to the fitted initial activity of $^{18}$Ne (introducing no free parameters),
(iii) an exponentially decaying component for the contaminant $^{18}$F in the beam, independent from the grow-in daughter component, with a free initial activity and fixed half-life, and
(iv) a fixed constant background rate in the gas counter.

Each cycle was fit individually to investigate the quality of the data and search for any spurious noise in the gas counter. The half-life results quoted in this article were obtained by summing all cycles across all of the runs and fitting this global data set in order to avoid the known bias introduced when averaging many lower-statistics half-life measurements [25].

### A. August 2013 experiment

During the first experiment, a total of 440 cycles were collected across 6 runs. The fixed, nonextendable dead times used for the two MCS modules were precisely measured to be 2.9856(57) and 3.9947(57) $\mu$s using the source-plus-pulser technique [32]. Once the data were dead time corrected and summed within a run, they were fit using the function described above. The background rates were fixed to values measured immediately following the experiment, as a function of both detector bias and discriminator threshold. A sample fit for one of the runs, with each of the components of the fit function, is shown in Fig. 1 while Fig. 2 shows the half-life as determined for each of the runs. The resulting half-life determined for $^{18}$Ne is 1.66424(62) s, where the uncertainty is purely statistical.

In order to investigate possible contaminants the beam was also delivered to the $8\pi$ $\gamma$-ray spectrometer [33,34]. A sample $\beta$-coincident $\gamma$-ray spectrum is shown in Fig. 3, where only $\gamma$ rays associated with the decay of $^{18}$Ne are visible. This method is, however, insensitive to contaminants that do not produce direct $\gamma$ radiation following $\beta$ decay, including $^{18}$F and $^{17}$F ($T_{1/2}$ = 64.49(16) s [35]) possibly delivered in our $A = 18$ beam as a $^{17}$F-H molecule. The $^{18}$F contaminant was included, with a free intensity, in the fits described above. We note, however, that the fit component labeled as $^{18}$F at $t = 0$ in Fig. 1 is consistent with the activity of $^{18}$F produced from the decays of $^{18}$Ne parent nuclei during the beam implantation and cooling period, and thus no $^{18}$F contaminant was delivered in the beam itself with the cold-transfer line.

Given the suppression of the $^{18}$F not resulting from decays of $^{18}$Ne to undetectable levels due to the cold-transfer line, one can readily assume that any potential $^{17}$F-H contamination would be suppressed to negligible levels. However, it is possible that the cold-transfer line would suppress the delivery of $^{18}$F and a possible $^{17}$F-H contaminant by different factors. Thus, the data were also refit, allowing the intensity of the $^{17}$F contaminant to be a free parameter, resulting in a nonphysical negative intensity of $(-64 \pm 225)$ $^{17}$F ions/s. Based on these

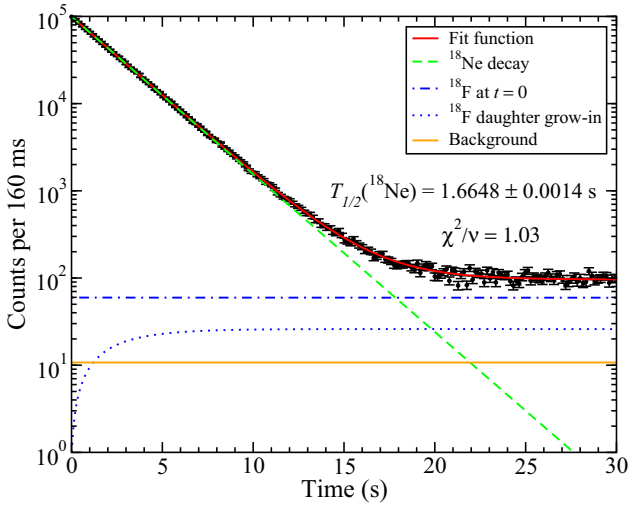


FIG. 1. (Color online) A typical dead-time-corrected decay curve with the fit function and components of the fit highlighted for the August 2013 experiment with the cold-transfer line between the target and ion source. The dead-time-corrected data from the 71 accepted cycles of this run have been summed prior to fitting. The background component (solid line, orange online) was determined from runs taken immediately following the experiment under the same conditions. Additionally, the $^{18}$F at $t = 0$ component is consistent with the $^{18}$F activity ($T_{1/2} = 109.73(2)$ min) produced from the decays of $^{18}$Ne parent nuclei during the beam implantation and cooling period, and thus no $^{18}$F contaminant was concluded to be in the beam itself.

analyses it was concluded that no significant $^{17}$F contaminant was present in the beam, in agreement with the previous $\gamma$-ray experiment performed using the same ISAC target and ion source combination [23].

In order to test for systematic effects, the data were grouped according to both the dead time applied to the data stream

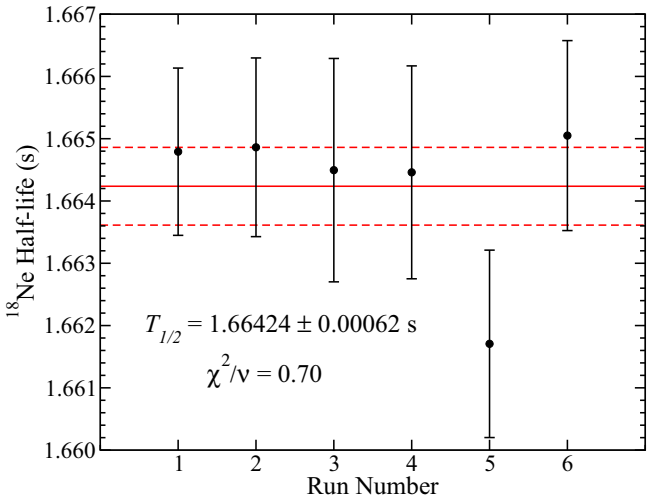


FIG. 2. (Color online) The half-life results obtained from each of the 6 runs taken in August 2013. The uncertainty quoted is statistical and the run-by-run reduced $\chi^2$ value is 0.70, indicating statistical consistency.

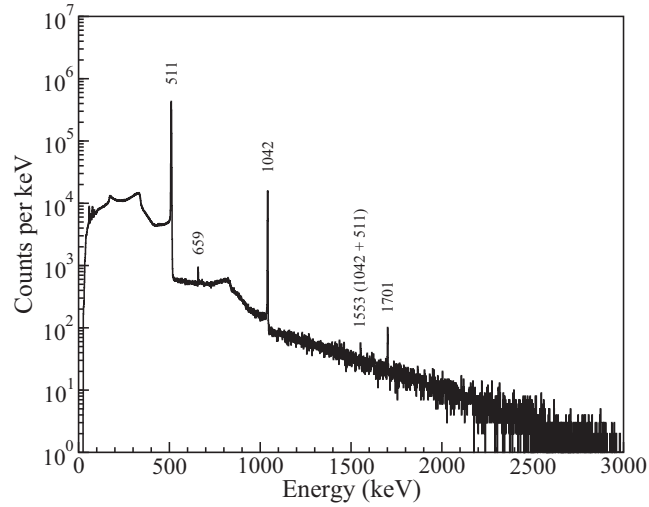


FIG. 3. A sample of the $\gamma$-ray spectrum in coincidence with $\beta$ particles collected with the $8\pi$ spectrometer in $\gamma$-singles mode. Only transitions following $^{18}$Ne $\beta$ decay were observed and are labeled by their energies in keV.

and the MCS module used to process the data. For all of these combinations, each of which contains the entire data set, the measured half-lives differed by less than $0.04\sigma$. The data were also grouped according to electronic settings for both the detector voltage (2700, 2750, or 2800 V) and discriminator threshold (70 or 95 mV), as shown in Fig. 4. The grouping for the threshold setting revealed $\chi^2/\nu = 1.03$ and resulted in a very modest inflation of the statistical uncertainty by a

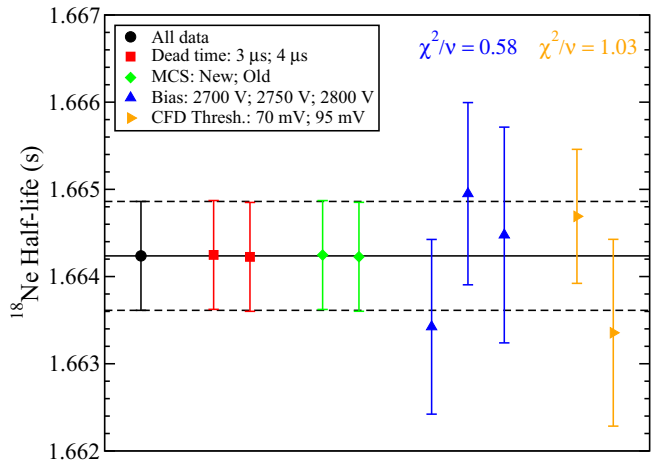


FIG. 4. (Color online) The half-life of $^{18}$Ne determined with the data grouped based on electronic setting. The dead time and MCS groupings each include the entire data set and therefore their unweighted average is taken as the "all data" result. The groupings for detector bias voltage and CFD threshold are independent subgrouping of the data and have their reduced $\chi^2$ values computed. Following the convention of the Particle Data Group the statistical uncertainty has been inflated by a small factor of $\sqrt{1.03} = 1.015$ in order to account for a potential systematic uncertainty associated with the CFD threshold.

TABLE I. Uncertainty contributions for the two gas counter measurements. For the entries labeled dead time and $^{18}$F half-life, the data were refit assuming the $\pm 1\sigma$ limits of these parameters and half of their difference was recorded as the associated systematic uncertainty. For the entry labeled background, either the background rates were fixed at their previously measured $\pm 1\sigma$ limits or a constant background contribution at a rate of 1 Hz was added, and their difference was added as a systematic uncertainty. The minimum number of counts required per cycle was changed to several different limits and the data were reanalyzed; the largest deviations between these values was added as a systematic uncertainty. Additionally, the potential effects of a beam contamination of $^{17}$F were investigated.

| | August 2013 | July 2014 |
|---|---|---|
| Statistical | 0.00062 s | 0.00043 s |
| Dead time | 0.00002 s | 0.00004 s |
| CFD threshold | 0.00011 s | |
| Background | $<10^{-6}$ s | $<10^{-6}$ s |
| $^{18}$F half-life | $<10^{-8}$ s | $<10^{-7}$ s |
| Cycle selection | 0.00010 s | 0.00007 s |
| $^{17}$F contamination | | 0.00025 s |
| Total | 0.00064 s | 0.00050 s |

factor of $\sqrt{\chi^2/\nu} = 1.015$, as per the prescription of the Particle Data Group [36]. As additional systematic investigations, the data were refit with the background, half-life of $^{18}$F, and the dead time each fixed at their $\pm 1\sigma$ limits, independently. The differences in central values from these six fits were treated as additional systematic uncertainties, all of which were entirely negligible compared to the $\pm 0.62$ ms statistical uncertainty. A further investigation of systematic uncertainty was the cycle selection criteria. Only those cycles with a minimum number of counts were kept in the final analysis to remove cycles with reduced or no transmission of $^{18}$Ne to the detector setup, resulting primarily from interruptions of the primary proton beam. Although those cycles during which a complete beam interruption occurred during implantation should be rejected, the exact threshold for the minimum number of counts in a cycle was subjective. Two different thresholds were applied: moderate (404 cycles, 96.7% of data retained) and relaxed (414 cycles, 98.3% of data retained). The final adopted analysis was with the moderate threshold, but the difference in half-lives measured between the two thresholds was added as an additional systematic uncertainty. All contributions to the final uncertainty are summarized in Table I. The resulting half-life of $^{18}$Ne was determined to be $1.66424(62)_{\text{stat.}}(15)_{\text{syst.}}$ s or 1.66424(64) s during the experiment performed in August 2013.

### B. July 2014 experiment

The second experiment followed very closely in procedure to the first experiment, with the differences being

(i) a newly constructed $4\pi$ gas counter was used,
(ii) the cold-transfer line between the production target and ion source was not used in the second experiment, and
(iii) the radioactive beam was delivered at 20 keV rather than 30 keV.

With the removal of the cold-transfer line a significant $^{18}$F contaminant of $1.1 \times 10^6$ ions/s was present in the beam and the activity due to this $^{18}$F was $\approx$100 times larger than the observed background rate in the gas counter. As the $^{18}$F activity ($T_{1/2} = 109.73(2)$ min [24]) is effectively constant over the 40-s decay measurements, it has an almost complete covariance with a constant background rate and thus no background component was used in the final fit of these data. Inclusion of a constant background rate fixed at the value of $\sim$1 Hz measured before and after the experiment was, however, included as a systematic test.

A total of 813 cycles were collected across 17 runs. The fixed, nonextendible dead times used for the two MCS modules were precisely measured to be 2.9798(34) and 3.9896(33) $\mu$s using the source-plus-pulser technique [32]. Following similar cycle selection criteria as described for the first experiment, the dead-time corrected data were summed within a run and fit using the function described above. A sample fit for one of the runs, with each of the components of the fit function, is shown in Fig. 5 while Fig. 6 shows the half-life as determined for each of the runs. The resulting $^{18}$Ne half-life is 1.66368(43) s, where the uncertainty is purely statistical.

In a previous $^{18}$Ne half-life experiment performed at the TRIUMF-ISAC facility also using a SiC target and FEBIAD ion source (and no cold-transfer line) [23], an upper limit was placed on the $^{17}$F beam contamination by optimizing a long implant and decay cycle and detecting the 511-keV $\gamma$-rays following $\beta^+$ annihilation. An upper limit on the ratio of $^{17}$F-H to $^{18}$F in the beam was determined to be 0.000152 with 90% confidence. In order to test for the effects of such a $^{17}$F contaminant in our beam, a component was added

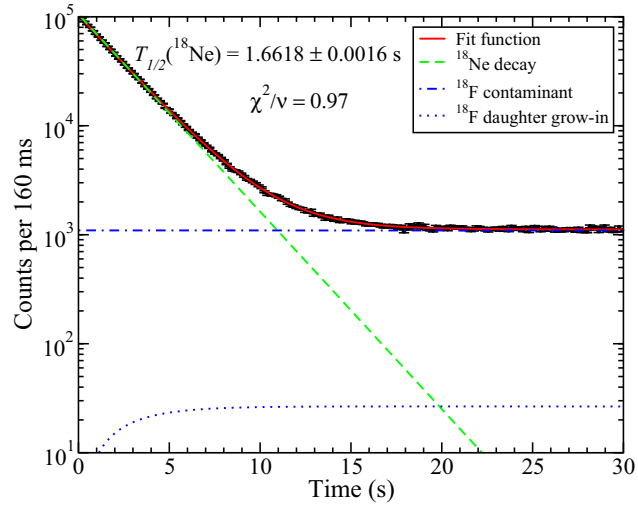


FIG. 5. (Color online) A typical dead-time-corrected decay curve with the fit function and components of the fit highlighted for the July 2014 experiment. The dead-time-corrected data from the 50 accepted cycles of this run have been summed prior to fitting. No constant background component was included, as the relative activity of $^{18}$F was increased after the removal of the cold-transfer line.

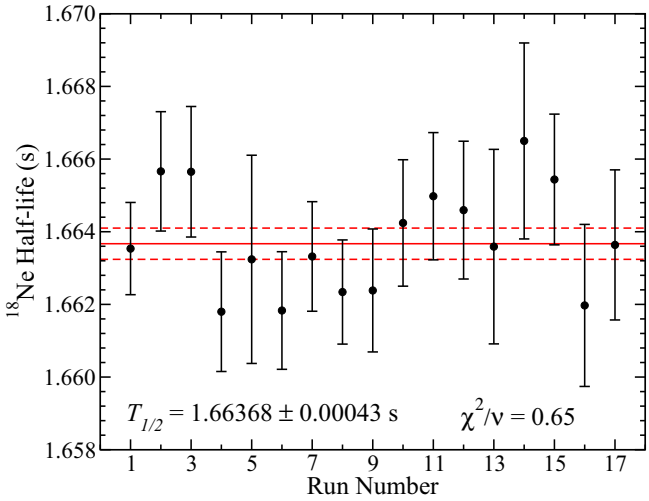


FIG. 6. (Color online) The half-life results obtained from each of the 17 runs taken in July 2014. The uncertainty quoted is statistical and the run-by-run reduced $\chi^2$ value of 0.65 suggests statistical consistency of the data.

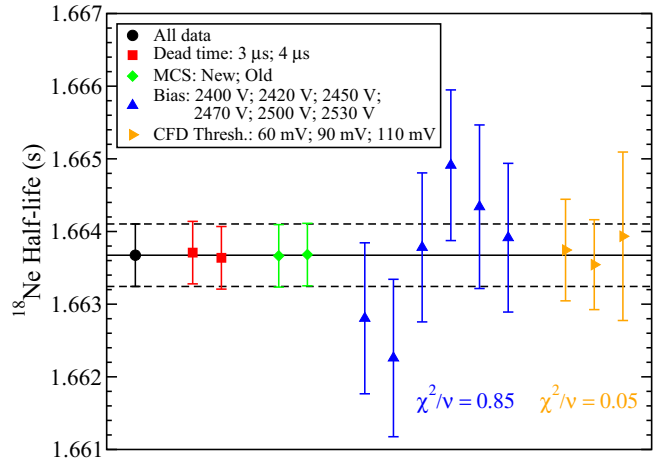


FIG. 7. (Color online) The half-life of $^{18}$Ne determined in the July 2014 experiment with the data grouped based on electronic setting. For the independent subgroupings by detector bias voltage and CFD threshold, the $\chi^2$ per degree of freedom was calculated and, since none were larger than 1, no inflation of the statistical uncertainty was applied.

to the fit function with a fixed $^{17}$F half-life and intensity corresponding to the $^{18}$F contaminant intensity multiplied by this upper limit on the $^{17}$F-H to $^{18}$F ratio. The resulting $^{18}$Ne half-life, 1.66343(43) s, was 0.6$\sigma$ shorter than when no $^{17}$F-H contaminant was included. Although there is no reason to suspect there is any contamination of $^{17}$F-H in the beam, which was identified in an earlier $^{18}$Ne experiment [37] at ISAC with an ECR ion source but has never been observed from the FEBIAD ion source used in this experiment, to be conservative we add a systematic uncertainty associated with the above upper limit of 170 $^{17}$F ions/s in the beam. We thus adopt a central value for the $^{18}$Ne half-life from the fit where no $^{17}$F-H contamination is included and add a systematic uncertainty of ±0.00025 s for the potential effects of $^{17}$F-H contamination in the beam.

As with the first experiment, a full set of systematic investigations was performed, including grouping the data according to electronic settings and several cycle selection criteria. A summary of the findings are outlined in Fig. 7 and Table I. Specifically, for the background, a fixed background rate of 1 count/s/cycle was added and the data were refit. The resulting $^{18}$Ne half-life differed by less than 1 ppm compared to when no constant background term was included, and thus no background component was included in the final analysis.

The half-life of $^{18}$Ne was thus determined to be $T_{1/2}$ = 1.66368(43)$_{\text{stat.}}$(26)$_{\text{syst.}}$ s or 1.66368(50) s using the new gas counter during the second experiment performed in July 2014.

### C. Investigation of rate-dependent effects

Although the analyses from the two independent MCS modules and two different dead-time settings were consistent during both experiments, additional tests were performed to search for potential rate-dependent effects on short time scales (100s of milliseconds to seconds). The data were reanalyzed with the leading channels (those with the highest rates) systematically removed, and are shown in Fig. 8 for both the August 2013 and July 2014 experiments. The data points in these plots are highly correlated, with each point containing all of the data to the right of it, and are thus not expected to be randomly distributed about an average value but rather follow slowly varying trends. No obvious trends are present that would suggest rate-dependent systematic effects biasing our $^{18}$Ne half-life results.

### D. Diffusion

Noble gases such as Ne are known [29,30] to diffuse rapidly in Mylar, with a room-temperature diffusion coefficient of approximately $2 \times 10^{-10}$ m$^2$/s [38]. Their diffusion when implanted in metallic foils is, however, very slow. Previous experiments with the $8\pi$ spectrometer at ISAC in which radioactive beams of noble gas ions were implanted at 30–60 keV into a tape transport system with an aluminum layer thickness of 2.51 mg/cm$^2$, or 9.4 $\mu$m (effectively infinite compared to the implantation depth of order ∼100 nm), found no detectable effects from diffusion [23,37,39]. These observations motivated the development of the new T-Tape system with a thick (17.2 $\mu$m) uniform Al layer used in the current experiments. Although the diffusion coefficients of noble gases in metals are known to be very small at room temperature there is very little quantitative information. Measurements [40] at ISAC of the diffusion of radioactive Xe implanted at 30 keV in thin metallic foils of Ta, Zr, and Pt that were resistively heated to ∼1000 °C yield impurity diffusion coefficients that, when extrapolated to room temperature, are in the range of $10^{-40}$ to $10^{-60}$ m$^2$/s. Similarly, the measured impurity diffusion of Ne in Ag in the 800–900 °C range [41], when extrapolated to room temperature, gives a diffusion coefficient of the order $10^{-48}$ m$^2$/s. Diffusion coefficients of

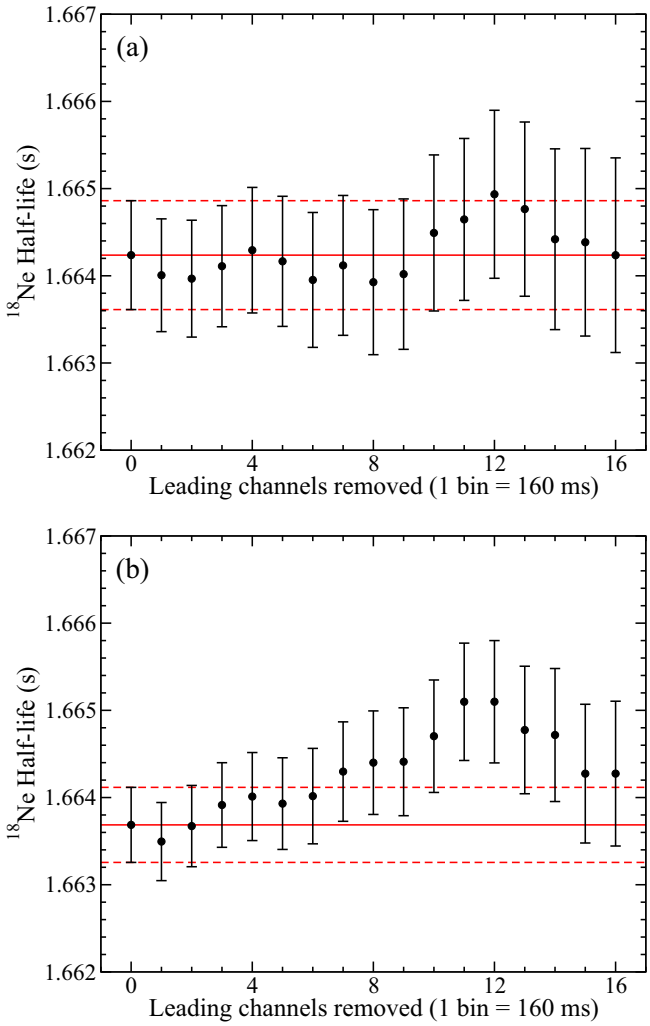


FIG. 8. (Color online) The half-life of $^{18}$Ne determined when leading high-rate channels are removed. Due to the highly correlated nature of these data with each point containing all of the data to the right of it, the points are not expected to be statistically scattered about a mean value. The data collected with the old gas counter in August 2013 is shown in panel (a) while the data collected with the new gas counter in July 2014 is shown in panel (b). In both cases, there is no clear systematic trend that would suggest the presence of rate-dependent effects.

this magnitude would have entirely negligible effects on the $^{18}$Ne half-life measurements presented in the current work. Such extrapolations of impurity diffusion coefficients over many orders of magnitude from the high-temperature (∼800–1000 °C) experiments where they can be readily measured to room temperature is, however, questionable and, at minimum, subject to very large uncertainties. In order to directly set upper limits on the room-temperature diffusion of Ne from the Al layer of our T-Tape system, we have investigated the longer lived ($T_{1/2} \approx 37$ s) $^{23}$Ne isotope and compared our half-life measurement to a previous precision measurement by Alburger [42], $T_{1/2} = 37.24(12)$ s, in which the $^{23}$Ne was confined in a liquid-nitrogen-cooled stainless-steel U-shaped tube filled with activated charcoal used to trap the samples and is thus not subject to diffusion effects.

The half-life of $^{23}$Ne was measured during the experiment performed in July 2014 using the same methods presented in Sec. III A. The 20-keV $^{23}$Ne beam was implanted into the T-Tape system at rates of approximately $8 \times 10^5$ $^{23}$Ne/s in two different cycling modes: (i) 2 s of beam on and 120 s of cooling (short implant) and (ii) 120 s of beam on and 290 s of cooling (long implant) before being moved to the center of the gas proportional counter. The cooling period was necessary to allow a contaminant of the shorter lived $^{23}$Mg ($T_{1/2} = 11.317(11)$ s [43]) in the $A = 23$ beam to decay. A longer lived contaminant with a half-life of approximately 2 h was also observed in the $A = 23$ beam. This is consistent with $^{18}$F ($T_{1/2} = 109.73(2)$ min [24]) that was likely delivered as a component of a doubly ionized $^{28}$Si$^{18}$F$^{2+}$ molecule formed in the SiC target at high temperatures as this molecule has the same $A/q$ as the $^{23}$Ne$^{+}$ ions to 1 part in 4000. In the short implantation runs, the $^{23}$Mg contaminant had a measurable activity during the decay period and was thus included in the fit function with a free intensity but fixed half- life, as shown in Fig. 9, while the intensity of the long-lived contamination was fixed at an upper limit determined from the measured activity during the long implant runs. Conversely, in the long implantation runs, the cooling time was sufficient to render the $^{23}$Mg activity negligible at the start of the counting period at the cost of introducing a larger component of the long-lived activity. The intensity of the long-lived contaminant was thus freed while the intensity of $^{23}$Mg was fixed at an upper limit determined from the measured $^{23}$Mg activity in the short implant cycles. The half-life of $^{23}$Ne was determined to be $T_{1/2} = 37.28(7)$ s for the short implant data and $T_{1/2} = 37.13(3)$ s for the long implant data. In Fig. 10, these results are compared to a recent $\gamma$-ray counting measurement in which the beam was implanted in an aluminized tape system ($T_{1/2} = 37.11(6)$ s [37]) and a measurement by Alburger in which the noble gas atoms were trapped in a stainless steel counting cell ($T_{1/2} = 37.24(12)$ s [42]). The consistency of these measurements suggests the absence of unknown systematic effects including diffusion. The weighted average half-life for $^{23}$Ne from these four measurements is 37.148(32) s, where the uncertainty includes a scaling factor of $\sqrt{1.73} = 1.3$ due to the reduced $\chi^2/\nu = 1.73$ for this set of measurements.

Taking a weighted average of the two $^{23}$Ne measurements performed in the current work, we obtain a half-life of $T_{1/2}(^{23}\text{Ne}) = 37.153(28)$ s, where the uncertainty is purely statistical. Comparing this result to the Alburger [42] measurement, which is free from diffusion effects, we obtain a half-life difference of $0.087 \pm 0.123$ s, which is consistent with zero and thus no measurable effects of $^{23}$Ne diffusion from our Al tape layer on the time scale of ∼10 min used in these experiments. However, by taking the 1 $\sigma$ upper limit on this half-life difference, i.e., $0.087 \pm 0.123 = 0.210$ s, we can directly set an *upper limit* on the diffusion rate of $^{23}$Ne from our Al tape layer.

Using the SRIM software package [44], the distributions of implanted Ne into aluminum were simulated for both 20 and 30 keV $^{18}$Ne and $^{23}$Ne beams, as shown in Fig. 11. The losses

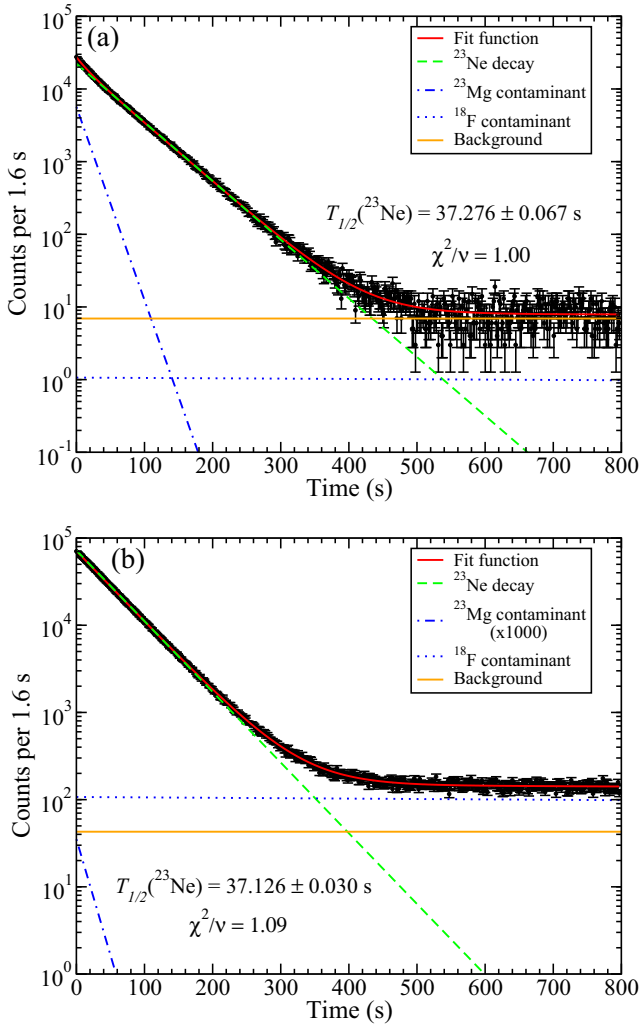


FIG. 9. (Color online) The fits to both cycling modes of the $^{23}$Ne data. (a) The short cycle data (2 s implant, 120 s cooling) which include a free intensity of the short-lived $^{23}$Mg and a fixed intensity of $^{18}$F set at its upper limit determined from the long cycle data. (b) The long cycle data (120 s implant, 290 s cooling) which includes a free intensity of the long-lived $^{18}$F contaminant and a fixed intensity of $^{23}$Mg set at its upper limit determined from the short cycle data.

associated with diffusion were modeled using a forward in time, central in space method [45] to numerically solve the 1D diffusion equation. These losses were simulated for a range of diffusion coefficients from $1 \times 10^{-20}$ to $1 \times 10^{-18}$ m$^2$/s in steps of $1 \times 10^{-20}$ m$^2$/s for the $^{23}$Ne experiments, and a selection of these can be seen in Fig. 12. Additionally, data sets were simulated using a nominal $^{23}$Ne half-life of 37.2 s to recreate the experimental data sets using the measured intensities of $^{23}$Ne, $^{23}$Mg, and $^{18}$F for each run and the data were fit using the functions described above. Taking the fractional losses from diffusion for each of the simulated diffusion coefficients, the $^{23}$Ne component was scaled on a bin-by-bin basis and the data were refit. This was used to establish an upper limit of $1.5 \times 10^{-19}$ m$^2$/s for the diffusion coefficient of $^{23}$Ne in Al, as can be seen in Fig. 13.

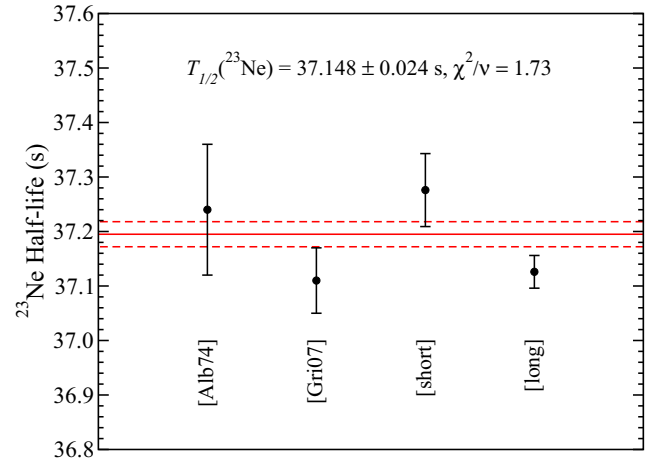


FIG. 10. (Color online) Comparison between previous high-precision $^{23}$Ne half-life measurements, including one where the sample was implanted in a stainless steel cell [42] and a $\gamma$-ray counting measurement [23], and the two $\beta$ counting measurements made during the July 2014 experiment with the long and short cycling times, respectively. The new world average $^{23}$Ne half-life is $37.148(24)_{\mathrm{stat.}}$, shown as dashed lines (red online), and the four measurements have $\chi^2/\nu = 1.73$.

It is worth noting that the upper limit we set on the diffusion coefficient for $^{23}$Ne in Al is ~5 orders of magnitude smaller than the value of $1.00 \pm 0.52_{(\mathrm{stat.})} \times 10^{-14}$ m$^2$/s quoted by Broussard et al. [46], which is obviously excluded by our data. Of course, their fit diffusion coefficient (see Fig. 2 of Ref. [46]) is consistent with zero at the $1.9\sigma$ level and already had negligible effects on their measurement, so the much more stringent upper limit established in the current work does not change the main conclusions of Broussard.

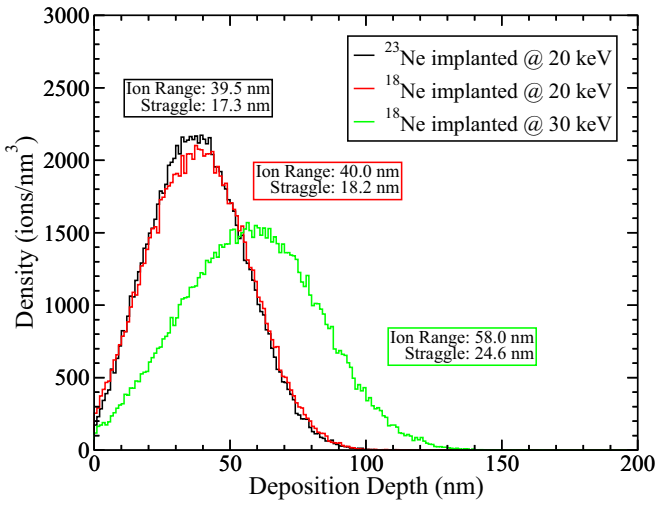


FIG. 11. (Color online) The implantation depth profile for 100 000 ions, as output by SRIM [44], for a $^{18}$Ne and $^{23}$Ne beam at 20 keV and a $^{18}$Ne beam at 30 keV into aluminum. The aluminum thickness of our tape is 17 200 nm and is thus effectively infinite in comparison to the characteristic Ne implantation depths.

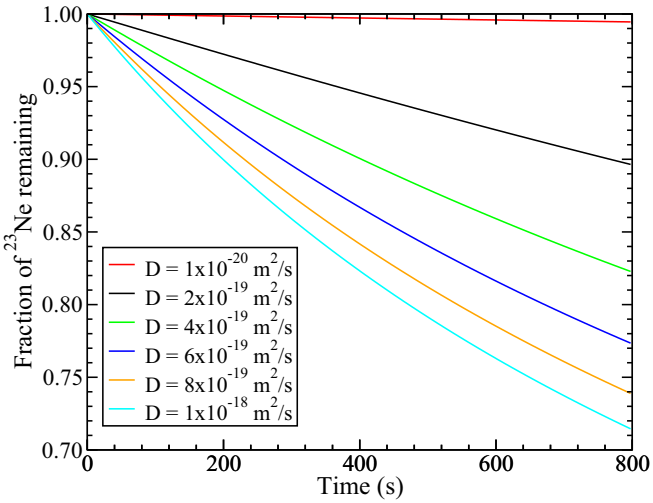


FIG. 12. (Color online) Simulations of the fraction of $^{23}$Ne remaining in the tape for different diffusion coefficients. Time $t = 0$ corresponds to the start of counting of the $^{23}$Ne in our gas counter (as in Fig. 9) and the simulation accounts for the diffusion of the $^{23}$Ne during the beam implantation and cooling periods prior to moving the sample into the gas counter.

In order to set an upper limit on the effects from diffusion on the $^{18}$Ne data sets, a similar simulation-based procedure was followed. A diffusion coefficient of $1.7 \times 10^{-19}$ m$^2$/s, which has been scaled by a factor of $\sqrt{23/18}$ to account for effects associated with mass, was used to simulate the fraction of losses associated with diffusion as a function of time for each of the 20- and 30-keV implantation profiles. Next, data sets were simulated to match the experimentally measured intensities of $^{18}$Ne and $^{18}$F for each run. The data were fit with no diffusion factor being applied, as well as when the $^{18}$Ne component was

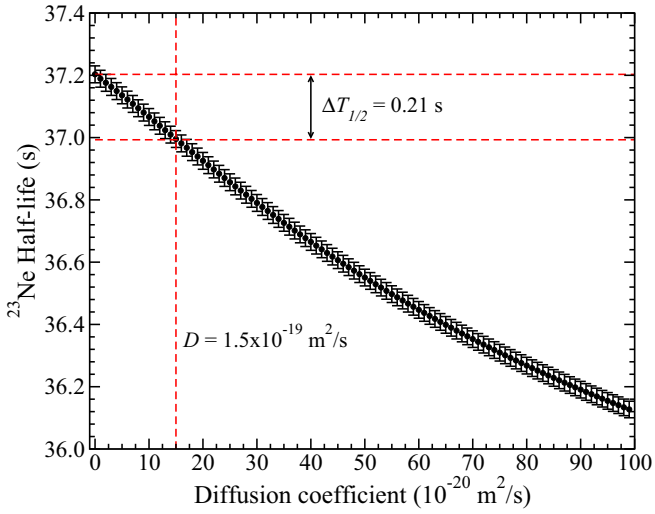


FIG. 13. (Color online) $^{23}$Ne half-life determined from a simulated data set after scaling the neon component bin by bin for losses associated with diffusion (see Fig. 12). A difference of 0.21 s is found for a diffusion coefficient of $1.5 \times 10^{-19}$ m$^2$/s, establishing an upper limit for the diffusion coefficient for Ne in Al.

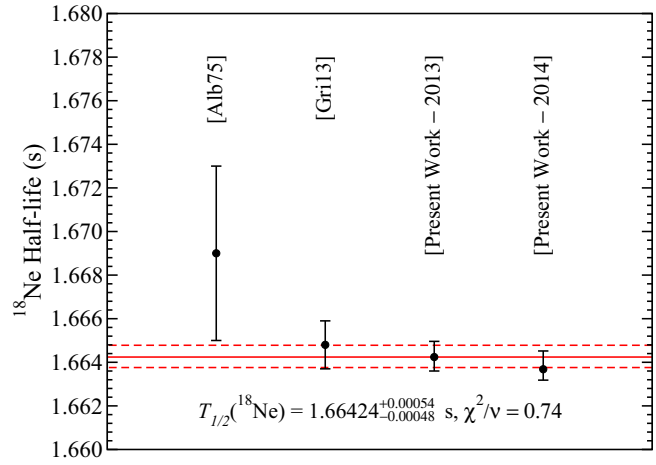


FIG. 14. (Color online) Comparison between previous high-precision $^{18}$Ne half-life measurements and the current results. The new world average $^{18}$Ne half-life, $T_{1/2} = 1.66424^{+0.00054}_{-0.00048}$ s, is shown by the solid and dashed lines.

scaled bin by bin, and a difference of 0.00033 s was found for $^{18}$Ne implanted at 30 keV and 0.00067 s for $^{18}$Ne implanted at 20 keV. These are taken to be systematic uncertainties, acting only in the positive direction, and are added in quadrature to the statistical and other systematic uncertainties established.

## IV. COMPARISON TO PREVIOUS MEASUREMENTS

The two independent $^{18}$Ne half-life measurements performed in the current work yield final values of $T_{1/2} = 1.66424^{+0.00072}_{-0.00064}$ s and $T_{1/2} = 1.66368^{+0.00084}_{-0.00050}$ s. As these two results are consistent with each other, we take a weighted average to obtain a final $^{18}$Ne half-life from the current work of $T_{1/2} = 1.66400^{+0.00057}_{-0.00048}$ s, where we used the methods outlined in Ref. [47] to average values with asymmetric uncertainties.

Comparing these results with previous measurements and adopting the procedure of retaining only measurements with uncertainties within an order of magnitude of the most precise measurement used in Ref. [1], two previous measurements satisfy this criteria: (i) a 1975 measurement by Alburger and Calaprice [48] and (ii) a recent measurement by $\gamma$-ray counting techniques repeated by Grinyer *et al.* [23], which we note incorporates, and thus supersedes, an earlier result reported in Ref. [37]. These two previous measurements are compared with our current results in Fig. 14 and yield a new world average half-life value for $^{18}$Ne of $T_{1/2} = 1.66424^{+0.00054}_{-0.00048}$ s, with a reduced $\chi^2$ value of 0.74.

## V. CONCLUSION

Two independent high-precision half-life measurements for $^{18}$Ne were performed, resulting in a weighted average of $T_{1/2} = 1.66400^{+0.00057}_{-0.00048}$ s from this work and a new world average $^{18}$Ne half-life value of $T_{1/2} = 1.66424^{+0.00054}_{-0.00048}$ s. The half-life of $^{18}$Ne is now determined to $\pm 0.034\%$ precision, comparable to the other precisely measured superallowed Fermi $\beta$ emitters. In order for the $^{18}$Ne $ft$ value to be

included among the high-precision cases, both the $Q$ value and branching ratio remain to be improved. Currently, the $Q$ value is measured to $\pm 0.02\%$ but a modern Penning trap measurement could reduce this source of uncertainty to negligible levels in the $^{18}$Ne $ft$ value determination. The $ft$ precision is currently limited by the branching ratio measurement, and improved precision for this branching ratio measurement [22] is essential for $^{18}$Ne to be included among the set of high-precision superallowed $ft$ values. This will provide a sensitive test of the nuclear-structure-dependent theoretical corrections for isospin symmetry breaking, as different models of the radial wave function give significantly different results in the case of $^{18}\text{Ne} \rightarrow {}^{18}$ F superallowed decay.

Half-life measurements for the heavier $^{23}$Ne were also made as part of an investigation of possible diffusion effects. Our results are consistent with negligible diffusion of Ne from our Al tape layer and the new world average $^{23}$Ne half-life is determined to be 37.148(32) s, an improvement by a factor of 1.7.

## ACKNOWLEDGMENTS

We thank Ed Zganjar and Randy Churchman for their efforts in designing, manufacturing, and installing the T-Tape transport system. This research has been partially supported by the Natural Sciences and Engineering Research Council of Canada and the CNRS (France) / TRIUMF (Canada) PICS program (Grant No. PICS 6207). TRIUMF receives federal funding via a contribution agreement through the National Research Council of Canada.

[1] J. C. Hardy and I. S. Towner, Phys. Rev. C **91**, 025501 (2015).
[2] J. C. Hardy and I. S. Towner, Ann. Phys. **525**, 443 (2013).
[3] I. S. Towner and J. C. Hardy, Rep. Prog. Phys. **73**, 046301 (2010).
[4] W. J. Marciano and A. Sirlin, Phys. Rev. Lett. **96**, 032002 (2006).
[5] W. E. Ormand and B. A. Brown, Phys. Rev. C **52**, 2455 (1995).
[6] H. Sagawa, N. Van Giai, and T. Suzuki, Phys. Rev. C **53**, 2163 (1996).
[7] I. S. Towner and J. C. Hardy, Phys. Rev. C **66**, 035501 (2002).
[8] I. S. Towner and J. C. Hardy, Phys. Rev. C **77**, 025501 (2008).
[9] G. A. Miller and A. Schwenk, Phys. Rev. C **78**, 035501 (2008).
[10] N. Auerbach, Phys. Rev. C **79**, 035502 (2009).
[11] H. Liang, N. V. Giai, and J. Meng, Phys. Rev. C **79**, 064316 (2009).
[12] G. A. Miller and A. Schwenk, Phys. Rev. C **80**, 064319 (2009).
[13] J. C. Hardy and I. S. Towner, Phys. Rev. C **79**, 055502 (2009).
[14] G. F. Grinyer, C. E. Svensson, and B. A. Brown, Nucl. Instrum. Methods A **622**, 236 (2010).
[15] I. S. Towner and J. C. Hardy, Phys. Rev. C **82**, 065501 (2010).
[16] W. Satuła, J. Dobaczewski, W. Nazarewicz, and T. R. Werner, Phys. Rev. C **86**, 054316 (2012).
[17] V. Rodin, Phys. Rev. C **88**, 064318 (2013).
[18] J. C. Hardy *et al.*, Phys. Rev. Lett. **91**, 082501 (2003).
[19] V. E. Iacob *et al.*, Phys. Rev. C **74**, 055502 (2006).
[20] H. I. Park *et al.*, Phys. Rev. Lett. **112**, 102502 (2014).
[21] B. Blank *et al.*, Eur. Phys. J. A **51**, 8 (2015).
[22] D. Nishimura (private communication).
[23] G. F. Grinyer *et al.*, Phys. Rev. C **87**, 045502 (2013).
[24] J. Han *et al.*, Appl. Radiat. Isot. **70**, 2581 (2012).
[25] V. T. Koslowsky, E. Hagberg, J. C. Hardy, G. Savard, H. Schmeing, K. S. Sharma, and X. J. Sun, Nucl. Instrum. Methods A **401**, 289 (1997).
[26] V. T. Koslowsky, E. Hagberg, J. C. Hardy, R. E. Azuma, E. T. H. Clifford, H. C. Evans, H. Schmeing, U. J. Schrewe, and K. S. Sharma, Nucl. Phys. A **405**, 29 (1983).
[27] G. F. Grinyer *et al.*, Phys. Rev. C **71**, 044309 (2005).
[28] P. Finlay *et al.*, Phys. Rev. Lett. **106**, 032501 (2011).
[29] U. C. Bergmann *et al.*, Nucl. Phys. A **714**, 21 (2003).
[30] V. E. Iacob and J. C. Hardy, Progress in Research, Texas A & M Cyclotron Institute Annual Report, V-42 (2011).
[31] G. F. Grinyer *et al.*, Nucl. Instrum. Methods A **579**, 1005 (2007).
[32] A. P. Baerg, Metrologia **1**, 131 (1965).
[33] C. E. Svensson *et al.*, Nucl. Instrum. Methods B **204**, 660 (2003).
[34] A. B. Garnsworthy and P. E. Garrett, Hyp. Int. **225**, 121 (2014).
[35] D. R. Tilley, H. R. Weller, and C. M. Cheves, Nucl. Phys. A **564**, 1 (1993).
[36] Particle Data Group, K. A. Olive *et al.*, Chin. Phys. C **38**, 090001 (2014).
[37] G. F. Grinyer *et al.*, Phys. Rev. C **76**, 025503 (2007).
[38] R. Ashu, R. M. Barreru, and D. G. Dalmer, Polymer **11**, 421 (1970).
[39] S. Triambak *et al.*, Phys. Rev. Lett. **109**, 042301 (2012).
[40] T. Warner *et al.*, Nucl. Instrum. Methods A **538**, 135 (2005).
[41] H. R. Glyde, J. Nucl. Mat. **23**, 75 (1967).
[42] D. E. Alburger, Phys. Rev. C **9**, 991 (1974).
[43] R. B. Firestone, Nucl. Data Sheets **108**, 1 (2007).
[44] J. F. Ziegler, M. D. Ziegler, and J. P. Biersack, Nucl. Instrum. Methods B **268**, 1818 (2010).
[45] P. J. Roach, *Computational Fluid Dynamics* (Hermosa, Albuquerque, NM, 1972).
[46] L. J. Broussard *et al.*, Phys. Rev. Lett. **112**, 212301 (2014).
[47] R. Barlow, arXiv:physics/0401042.
[48] D. E. Alburger and F. P. Calaprice, Phys. Rev. C **12**, 1690 (1975).